RSC Advances

ROYAL SOCIETY OF CHEMISTRY

www.rsc.org/advances

A turn-on fluorescent pyrene-based chemosensor for Cu(II) with live cell

application

Parthiban Venkatesan, Shu-Pao Wu*

Department of Applied Chemistry, National Chiao Tung University, Hsinchu 300, Taiwan

*Corresponding author.

Tel.: +886-3-5712121-ext56506; Fax: +886-3-5723764

E-mail: spwu@mail.nctu.edu.tw

Abstract:

A pyrene-based fluorescent sensor (**PHP**) was synthesized for Cu(II) detection. It had high selectivity towards Cu^{2+} ions *via* photoinduced electron transfer (PET) based fluorescence enhancement. In the presence of Cu^{2+}, **PHP** provided significant blue emission, while Ag^+, Al^{3+}, Ca^{2+}, Cd^{2+}, Co^{2+}, Cr^{3+}, Fe^{2+}, Fe^{3+}, Hg^{2+}, Mg^{2+}, Mn^{2+}, Ni^{2+}, Pb^{2+}, and Zn^{2+} metal ions produced only minor changes in fluorescence spectra. The association constant (K_a) for Cu^{2+} binding to **PHP** had a value of 1.0×10^4 M^{-1}. The maximum emission change induced by Cu^{2+} binding to the chemosensor **PHP** was observed over the pH range 5.0–10.0. Confocal fluorescence microscopy imaging using RAW264.7 cells showed that **PHP** can be used as an effective fluorescent probe for detecting Cu^{2+} in living cells.

1. Introduction

The development of selective and sensitive chemosensors for biologically relevant cations and anions has gained much attention in the past decades because they played crucial roles in clinical and environmental analysis.[1-3] Among essential metal ions, copper is the third most abundant essential transition metal ion in the human body. Copper ion is used as a cofactor for electron transport, or as a catalyst in oxido-reduction reactions in many proteins. As copper ion also reacts with dioxygen to form reactive oxygen species (ROS) that can damage lipids, nucleic acids and proteins, their cellular toxicity is connected to serious neurodegenerative diseases, including Menkes and Wilson disease,[4-7] Alzheimer's disease, and prion disease.[8] Due to its extensive applications in our daily lives, copper is also a common metal pollutant. The limit for copper in drinking water, as set by the US Environmental Protection Agency (EPA) is 1.3 ppm (20 μM).

The development of fluorescent chemosensors for Cu^{2+} detection has been an important research topic. Because Cu^{2+} is known as a fluorescence quencher, most fluorescent chemosensors detect Cu^{2+} by the fluorescence quenching processes, which involve charge or energy transfer mechanisms.[9] Due to sensitivity issues, fluorescent sensors with a turn-off process offer poor sensitivity for metal ion detection compared to fluorescence enhancement sensors.[10-29] This paper reports on a newly designed pyrene-based fluorescence enhancement chemosensor for Cu^{2+} that is based on photoinduced electron transfer (PET). Cu^{2+} binding with the chemosensor blocks the PET mechanism and greatly enhances the fluorescence of the pyrene moiety.

In this report, a pyrene based fluorescent probe (**PHP**) with hydrazinylpyridine moiety[30] was developed for the detection of Cu^{2+} ions. The chemosensor **PHP** exhibits

weak fluorescence due to fluorescence quenching by photo-induced electron transfer from nitrogen lone pairs onto pyrene. The binding of a metal ion chemosensor blocks the PET mechanism, resulting in significant enhancement in pyrene fluorescence. The metal ions Ag^+, Al^{3+}, Ca^{2+}, Cd^{2+}, Co^{2+}, Cr^{3+}, Cu^{2+}, Fe^{2+}, Fe^{3+}, Hg^{2+}, Mg^{2+}, Mn^{2+}, Ni^{2+}, Pb^{2+}, and Zn^{2+} were tested with the fluorescent probe **PHP**. Selectivity testing revealed that Cu^{2+} causes a visible color change in **PHP**, from light yellow or colorless, and a blue emission on ligation to **PHP**; no other tested ions produced a significant color change. Furthermore, chemosensor **PHP** is cell membrane permeable and can be used for the detection of Cu^{2+} in living cells.

2. Experimental

2.1 Materials and Instrumentation.

All solvents and reagents were obtained from commercial sources and used without further purification. UV/Vis spectra were recorded on an Agilent 8453 UV/Vis spectrometer. Fluorescence spectra measurements were performed on a Hitachi F-7000 fluorescence spectrophotometer. NMR spectra were obtained on a Bruker DRX-300 and Agilent Unity INOVA-500 NMR spectrometer. Fluorescent images were taken on a Leica TCS SP5 X AOBS Confocal Fluorescence Microscope.

2.2 Synthesis of (Z)-2-(2-(pyren-1-ylmethylene)hydrazinyl)pyridine

1-Pyrenecarboxaldehyde (230 mg, 1.0 mmol) and 2-hydrazinylpyridine (182 mg, 1.1 mmol) were added to a 10 mL ethanol solution. The reaction mixture was refluxed for 12 hr. The resulting precipitate was collected by filtration and then purified by column chromatography (ethyl acetate: hexane = 1:1) to give 1 as a bright yellow solid. Yield:

336 mg (89%). Melting point: 234-236 °C. ^{1}H NMR (300 MHz, DMSO-d$_6$) : δ 11.11 (s, 1H), 9.13 (s, 1H), 8.70 (d, 1H, J = 9.3 Hz), 8.61 (d, 1H, J = 8.4 Hz), 8.31 (m, 4H), 8.17-8.21 (m, 3H), 8.10 (t, 1H, J=7.5Hz),7.7(t,1H, J=6.9Hz), 7.34 (d, 1H, J = 8.4Hz,), 6.83 (t, 1H, J = 5.1 Hz,); ^{13}C NMR (75 MHz, DMSO-d$_6$): 157.4, 148.4, 138.6, 137.7, 131.5, 131.3, 130.8, 128.8, 128.7, 128.1, 128.1, 127.9, 127.0, 126.2, 125.8, 124.8, 124.5, 124.4, 122.2, 115.7, 107.0; MS(ESI): m/z = 322.2 ([M+H]$^+$); HRMS (ESI): calcd. for C$_{22}$H$_{16}$N$_3$ ([M+H]$^+$) 322.1344; found 322.1345. FTIR (cm^{-1}): 3200, 2997, 1595, 1444, 1329, 1139, 994, 906, 843.

2.3 Cation selection study by fluorescence spectroscopy.

PHP (10 μM) was added with different cations (1 mM). All spectra were measured in 1.0 mL acetonitrile-PBS buffer (0.01M, pH-7.4) (v/v = 4:6). The light path length of cuvette was 1.0 cm.

2.4 Determination of the binding stoichiometry and the stability constants K$_a$ of Cu^{2+} binding in chemosensor PHP.

The binding stoichiometry of **PHP**-Cu^{2+} complexes was determined by Job plot experiments. The emission at 389 nm was plotted against molar fraction of **PHP** under a constant total concentration. The total concentration of sensor and Cu^{2+} ion was 200 μM. The molar fraction at maximum emission intensity represents the binding stoichiometry of the **PHP**-Cu^{2+} complexes. The maximum emission intensity was reached at a molar fraction of 0.5. The association constants K_a of **PHP**-Cu^{2+} complexes were determined by the Benesi–Hilderbrand equation:[31]

$$1/\Delta F = 1/\Delta F_{sat} + 1/(\Delta F_{sat}\ K_a[Cu^{2+}])\ (1)$$

where ΔF is the fluorescence intensity difference at 389 nm and ΔF_{sat} is the maximum fluorescence intensity difference at 389 nm. The association constant K_a was evaluated graphically by plotting $1/\Delta F$ against $1/[\,Cu^{2+}]$. Data were linearly fitted according to eqn (1) and the K_a value was obtained from the slope and intercept of the line.

2.5 The pH dependence on the reaction of Cu^{2+} with PHP by fluorescence spectroscopy

PHP (10 μM) was added with Cu^{2+} (10 μM) in 1.0 mL acetonitrile-PBS buffer (0.01M, pH-7.4) (v/v = 4:6). The buffers were: pH 3 ~ 4, KH_2PO_4/HCl; pH 4.5 ~ 6, KH_2PO_4/NaOH; pH 6.5 ~ 8.5, HEPES; pH 9 ~ 10, Tris-HCl.

2.6 Cell culture for RAW264.7 Macrophages

The cell line RAW264.7 was provided by the Food Industry Research and Development Institute (Taiwan). RAW264.7 cells were cultured in Dulbecco's modied Eagle's medium (DMEM) supplemented with 10% fetal bovine serum (FBS) at 37 °C under an atmosphere of 5% CO_2. Cells were plated on 18 mm glass coverslips and allowed to adhere for 24 h.

2.7 Cytotoxicity assay

The methyl thiazolyl tetrazolium (MTT) assay was used to measure the cytotoxicity of **PHP** in RAW264.7 cells. RAW264.7 cells were seeded into a 96-well cell-culture plate. Various concentrations (10, 20, 30, 40, 50 μM) of PHP were added to the wells. The cells were incubated at 37 °C under 5% CO_2 for 24 h. 10 μL MTT (5 mg/mL) was added to each well and incubated at 37 °C under 5% CO_2 for 4 h. Remove the MTT solution and yellow precipitates (formazan) observed in plates were dissolved in 200 μL DMSO and

25 μL Sorenson's glycine buffer (0.1 M glycine and 0.1 M NaCl). Multiskan GO microplate reader was used to measure the absorbance at 570 nm for each well. The viability of cells was calculated according to the following equation:

Cell viability (%) = (mean of absorbance value of treatment group) / (mean of absorbance value of control group).

2.8 Fluorescence imaging of PHP

Experiments to assess Cu^{2+} uptake were performed in PBS with 10 μM $CuCl_2$. Treated with the cells with 2 μL of 10 mM metal ions (final concentration: 10 μM) dissolved in sterilized PBS (pH 7.4) and incubated for 30 min at 37℃. The treated cells was washed PBS (3×2 mL) to remove remaining metal ions. Culture media (2 mL) was added to the cell culture, which was treated with a 10 mM solution of **PHP** (2μL; final concentration: 10 μM) dissolved in DMSO. The samples were incubated at 37℃ for 30 min. The culture media was removed, and the treated cells were washed with PBS (3×2 mL) before observation. Confocal fluorescence imaging of cells was performed with a Leica TCS SP5 X AOBS Confocal Fluorescence Microscope (Germany), and a 63x oil-immersion objective lens was used. The cells were excited with a white light laser at 346 nm, and emission was collected at 380±10 nm.

2.9 Computational methods

Quantum chemical calculations based on density functional theory (DFT) were carried out using a Gaussian 09 program. The ground-state structures of **PHP** and **PHP**–Cu^{2+} complexes were computed using the density functional theory (DFT) method with functional B3LYP. The 6-31G basis set was assigned to nonmetal elements (C, H, and N).

For the **PHP**–Cu^{2+} complex, the LanL2DZ basis set was used for Cu^{2+}, whereas the 6-31G basis set was used for other atoms.

3. Results and discussion

3.1 Synthesis of PHP

Chemosensor **PHP** was synthesized by the reaction of 1-pyrenecarboxaldehyde and 2-hydrazinylpyridine to form an imine bond between hydrazinylpyridine and pyrene (Scheme 1). **PHP** is yellow and has an absorption band at 383 nm, which is red-shifted by 50 nmfrom the pyrene absorption band at 335 nm. This is due to longer conjugated double bonds in chemosensor **PHP**. Chemosensor **PHP** exhibits a weak fluorescence (Φ = 0.001) compared to pyrene (Φ= 0.6-0.9). This observation can be attributed to fluorescence quenching by photoinduced electron transfer from electron lone pairs on nitrogen onto pyrene.

3.2 Cation-sensing properties

The sensing properties of **PHP** were investigated by monitoring the absorption and emission behaviors upon addition of several metal ions Ag^+, Al^{3+}, Ca^{2+}, Cd^{2+}, Co^{2+}, Cr^{3+}, Cu^{2+}, Fe^{2+}, Fe^{3+}, Hg^{2+}, Mg^{2+}, Mn^{2+}, Ni^{2+}, Pb^{2+}, and Zn^{2+}. Cu^{2+} caused a visible color change in **PHP,** from light yellow to colorless, and had a blue emission (Fig. 1); other metal ions only caused a minor change in the absorption and emission spectra (see Figure S5 in the supplementary data). During Cu^{2+} titration with **PHP**, the absorbance at 385 nm decreased in intensity, and a new band centered at 343 nm appeared (Fig. 2a). The color change from light yellow to colorless (Fig. 1) clearly indicates the 42-nm blue shift. The new band at 343 nm is close to the absorption band of pyrene at 335 nm. This observation suggests that Cu^{2+} binding with chemosensor **PHP** blocks conjugation between the

double bonds, resulting in a shorter absorption wavelength. In addition, Cu^{2+} titration with chemosensor **PHP** results in a new emission band centered at 389 nm (Fig. 2b). After adding 1.5 molar equivalents of Cu^{2+}, the emission intensity reached a maximum. The quantum yield of the new emission band was 0.56, which was 560-fold that of chemosensor **PHP** at 0.001. Cu^{2+} was the only metal ion of those we tested that readily binds with chemosensor **PHP** to yield a significant fluorescence enhancement, suggesting application for the highly selective detection of Cu^{2+} ion.

To understand the binding stoichiometry of the **PHP**-Cu^{2+} complex, Job plot experiments were carried out. In Fig. 3, the emission intensity at 389 nm is plotted against the molar fraction of chemosensor **PHP** at a constant total concentration of 50 μM. Maximum emission intensity was reached for a molar fraction of 0.50, indicating that one Cu^{2+} ion binds with one chemosensor **PHP** molecule. The formation of a **PHP**-Cu^{2+} complex was confirmed by ESI-MS, in which the peak at $m/z = 383.05$ indicates a 1:1 stoichiometry for the $[(\textbf{PHP}\text{-}H^{+})+Cu^{2+}]$ complex (See Figure S5 in the supplementary data). The association constant K_a was evaluated graphically by plotting $1/(F\text{-}F_0)$ against $1/[\,Cu^{2+}]$ (Fig. 4). The data was linearly fit according to the Benesi–Hilderbrand equation, and the K_a value was obtained from the slope and intercept of the line. The K_a value of the **PHP**-Cu^{2+} complex was 1.0×10^{4} M^{-1}. The detection limit of **PHP** as a fluorescent sensor for the analysis of Cu^{2+} was determined from the plot of fluorescence intensity as a function of the concentration of Cu^{2+} (see Figure S7 in the supporting information). **PHP** was found to have a detection limit of 0.04 μM, which is reasonable for the detection of micromolar concentrations of Cu^{2+}.

To further confirm the high selectivity of **PHP** for Cu^{2+} detection, a competitive experiment of coexisting ions was performed, in which **PHP** (10 μM) was examined with 40 μM of various metal ions Ag^+, Al^{3+}, Ca^{2+}, Cd^{2+}, Co^{2+}, Cr^{3+}, Fe^{2+}, Fe^{3+}, Hg^{2+}, Mg^{2+}, Mn^{2+}, Ni^{2+}, Pb^{2+}, and Zn^{2+}. Cu^{2+}, followed by the addition 20 μM of Cu^{2+} ions. As shown in Fig.5, the fluorescence enhancement observed for most of the mixtures of Cu^{2+} with other metal ions was similar to that caused by Cu^{2+} alone. These observations indicated that most of the other metal ions do not interfere with the binding of **PHP** to Cu^{2+}.

A pH titration of **PHP** was carried out to determine a suitable pH range for Cu^{2+} detection. As depicted in Fig. 6, the emission intensities of metal-free **PHP** are very low at all pH values. After mixing **PHP** with Cu^{2+}, the emission intensity at 389 nm increased in the pH range of 4.0–10.0. At pH <5, the emission intensity is bigger due to higher emission from the protonation form of the PHP-Cu^{2+} complex. These observations indicated that the **PHP**–Cu^{2+} complex is essentially pH-insensitive over the range 4.0 to 10.0, indicating that the fluorescence of the **PHP**–Cu^{2+} complex is stable over a wide pH range.

To understand the reversibility of the **PHP**-Cu^{2+} complex, a reversibility experiment was carried out with the addition of EDTA, which has a strong binding ability towards Cu^{2+}. Fig. 7 shows that the introduction of EDTA can immediately decrease the emission intensity. Further addition of Cu^{2+} can restore the fluorescent state. This cycle (Cu^{2+}-EDTA) can be carried out four times. This regeneration indicates that **PHP** can be reused with proper treatment.

In order to investigate Cu^{2+} binding to **PHP**, density functional theory (DFT) calculations were employed. Due to the 1:1 ligand-to-metal complex determined by Job

plot, the chemosensor **PHP** with and without Cu^{2+} was subjected to energy optimization at the B3LYP hybrid functional with the LanL2DZ basis set. The lowest energy conformation for **PHP**-Cu^{2+} has one chemosensor **PHP** molecule binding with one Cu^{2+} ion, where the Cu^{2+} ion is bonded by two nitrogens at a distance of 2.06, and 2.03 Å, respectively (Fig. 8).

To investigate the mechanism of Cu^{2+}-detection, density functional theory (DFT) calculations were also employed using the Gaussian 09 software package. As shown in Fig. 9, the highest occupied molecular orbital (HOMO) of **PHP** (electron donor) is close to that of the fluorophore pyrene (electron acceptor); the HOMO energy level (−4.93 eV) of the binding moiety is higher than that of pyrene (−5.59 eV). Consequently, when the pyrene moiety is excited by light, electron transfer from the binding moiety to the pyrene is energetically allowed. Hence, the pyrene fluorescence is quenched by the PET process (Φ < 0.01). In contrast, upon the binding of **PHP** to Cu^{2+}, the HOMO energy level of the binding moiety decreases to below that of pyrene; the PET process is thus forbidden and pyrene fluorescence reemerges.

3.3 Cell imaging of PHP

The potential of **PHP** for imaging Cu^{2+} in living cells was investigated next. First, an MTT assay with a RAW 264.7 cell line was used to determine the cytotoxicity of **PHP**. In Fig. 10, the cellular viability was estimated to be greater than 80% after 24 h, which indicates that **PHP** (< 30 μM) has low cytotoxicity. Cell images were further obtained using a confocal fluorescence microscope. When RAW 264.7 cells were incubated with **PHP** (10 μM), no fluorescence was observed (Fig. 11a). After treatment with Cu^{2+}, bright blue fluorescence was observed in the RAW 264.7 cells (Fig. 11b). An overlay of

fluorescence and bright-field images showed that the fluorescence signals were localized in the intracellular area, indicating a subcellular distribution of Cu^{2+} and good cell-membrane permeability of **PHP**.

4. Conclusion:

In conclusion, we have developed a new fluorescent probe **PHP** for a rapid, highly selective and sensitive response to Cu^{2+} ions over the other metal ions via a fluorescent turn-on response. An extremely suitable pH range was established for Cu^{2+} detection with **PHP** between 4.0 – 9.5. Further, the DFT calculation demonstrated a fluorescent turn-on mechanism in which the photo induced electron transfer (PET) from the donor to pyrene is suppressed by Cu^{2+} binding. Most importantly, the chemosensor **PHP** can potentially be applied in fluorescence imaging of living cells. This pyrene-based chemosensor **PHP** has low cytotoxicity and can therefore be used for detecting Cu^{2+} in living cells.

Notes and references

[a] Department of Applied Chemistry, National Chiao Tung University, Hsinchu, Taiwan 300, Republic of China E-mail: spwu@mail.nctu.edu.tw;

Fax: +886-3-5723764; Tel: +886-3-5712121 ext. 56506

1 X. Li, X. Gao, W. Shi and H. Ma, *Chem. Rev.,* 2014, **114**, 590-659.

2 K. P. Carter, A. M. Young and A. E. Palmer, *Chem. Rev.*, 2014, **114**, 4564-4601.

3 M. Formica, V. Fusi, L. Giorgi and M. Micheloni, *Coord. Chem. Rev.*, 2012, **256**, 170-192.

4 K. J. Barnham, C. L. Masters and A. I. Bush, *Nat. Rev. Drug Discov.*, 2004, **3**, 205-214.

5 L. M. Gaetke and C. K. Chow, *Toxicology*, 2003, **189**, 147-163.

6 D. J. Waggoner, T. B. Bartnikas and J. D. Gitlin, *Neurobiol. Dis.*, 1999, **6**, 221-230.

7 P. Zatta and A. Frank, *Brain Res. Rev.*, 2007, **54**, 19-33.

8. E. Gaggelli, H. Kozlowski, D. Valensin and G. Valensin, *Chem. Rev.*, 2006, **106**, 1995-2044.

9. H. S. Jung, P. S. Kwon, J. W. Lee, J. Kim, C. S. Hong, J. W. Kim, S. Yan, J. Y. Lee, J. W. Lee, T. Joo and S. Kim, *J. Am. Chem. Soc.*, 2009, **131**, 2008–2012.

10 S. Kaur and S. Kumar, *Chem. Comm.*, 2002, 2840–2841

11 S. Kumar, P. Singh and S. Kaur, *Tetrahedron*, 2007, **63**, 11724–11732

12 M. P. Algi, Z. Oztas and F. Algi, *Chem. Commun.*, 2012, **48**, 10219–10221.

13 J. Jo, H. Y. Lee, W. Liu, A. Olasz, C. Chen and D. Lee, *J. Am. Chem. Soc.*, 2012, **134**, 16000–16007.

14 K. Li, N. Li, X. Chen and A. Tong, *Anal. Chim. Acta*, 2012, **712**, 115-119.

15 Z. Liu, C. Zhang, X. Wang, W. He, and Z. Guo, *Org. Lett*. 2012, **14**, 4378-4381.

16 J. Fan, X. Liu, M. Hu, H. Zhu, F. Song and X. Peng, *Anal. Chim. Acta*, 2012, **735**, 107-113.

17 J. Liu, L. Lin, X. Wang, S. Lin, W. Cai, L. Zhang and Z. Zheng, *Analyst*, 2012, **137**, 2637-2642.

18 C. Chou, S. Liu and S. Wu, *Analyst*, 2013, **138**, 3264-3270

19 J. Yeh, W. Chen, S. Liu and S.-P. Wu, *New J. Chem*., 2014, **38**, 4434-4439.

20 P. Singh, L. S. Mittal, S. Kumar, G. Bhargava and S. Kumar, *J. Fluoresc.*, 2014, **24**, 909–915

21 P. Singh, R. Kumar and S. Kumar, *J. Fluoresc.*, 2014, **24**, 417–424

22 B. Muthuraj, S. R. Chowdhury, S. Mukherjee, C. R. Patra and P. K. Iyer, *RSC Adv*., 2015, **5**, 28211 28218.

23 S. Chemate and N. Sekar, *RSC Adv*., 2015, **5**, 27282-27289.

24 S. R. Patil, J. P. Nandre, P. A. Patil, S. K. Sahoo, M. Devi, C. P. Pradeep, Y. Fabiao, L. Chen, C. Redshaw and U. D. Patil, *RSC Adv*., 2015, **5**, 21464-21470.

25 G. Li, F. Tao, H. Wang, L. Wang, J. Zhang, P. Ge, L. Liu, Y. Tong and S. Sun, *RSC Adv*., 2015, **5**, 18983-18989.

26 S. Pathak, D. Das, A. Kundu, S. Maity, N. Guchhait and A. Pramanik, *RSC Adv*., 2015, **5**, 17308-17318.

27 G. Singh, J. Singh, S. S. Mangat, J. Singh and S. Rani, *RSC Adv*., 2015, **5**, 12644-12654.

28 D. Sarkar, A. K. Pramanik and T. K. Mondal, *RSC Adv*., 2015, **5**, 7647-7653.

29 L. Wenfeng, M. Hengchang, L. con, M. Yuan, Q. Chunxuan, Z. Zhonwei, Y. Zengming, C. Haiying and L. ziqiang, *RSC Adv*., 2015, **5**, 6869-6878.

30 M. Ucuncu and M. Emrullahoglu, *RSC Adv*., 2015, **5**, 30522–30525

31 H. A. Benesi and J. H. Hildebrand, *J. Am. Chem. Soc.,* 1949, **71**, 2703–2707.

Figure and scheme captions

1. Scheme 1. Synthesis of **PHP**

2. Fig. 1. (a) Color and (b) fluorescence changes of **PHP** (100 μM) after addition of various metal ions (100 μM) in CH_3CN/H_2O (v/v = 4:6, 10 mM PBS, pH 7.4) solution.

3. Fig. 2. (a) Absorption change and (b) fluorescence response of **PHP** (10 μM) to various equivalents of Cu^{2+} in CH_3CN/H_2O (v/v = 4:6, 10 mM PBS, pH 7.4) solution.

4. Fig. 3. Job plot of the Cu^{2+}-**PHP** complexes in CH_3CN/H_2O (v/v = 4:6, 10 mM PBS, pH 7.4) solution. The total concentration of **PHP** and Cu^{2+} was 50 μM. The excitation wavelength was 346 nm.

5. Fig. 4 Binding constant for titration of Cu^{2+} (0.1 to 1.0 eq) against ratio of fluorescence response for **PHP** (10 μM) in CH_3CN/H_2O (v/v = 4:6, 10 mM PBS, pH 7.4) solution. The excitation wavelength was 346 nm.

6. Fig. 5. Fluorescence response of **PHP** (10 μM) to Cu^{2+} (20 μM) or 100 μM of other metal ions (the black bar portion) and to the mixture of other metal ions (40 μM) with Cu^{2+} (20 μM) (the gray bar portion) in CH_3CN/H_2O (v/v = 4:6, 10 mM PBS, pH 7.4) solution.

7. Fig. 6. Fluorescence response (389 nm) of free **PHP (**10 μM) and after addition of Cu^{2+} (10 μM) in CH_3CN/H_2O (v/v = 4:6, 10 mM PBS) solutions as a function of various pH values. The excitation wavelength was 346 nm.

8. Fig. 7. Reversible binding of Cu^{2+} with **PHP**. Fluorescence spectra of (a) **PHP**, (b) **PHP** in the presence of Cu^{2+} (10 μM), and (c) probe in the presence of Cu^{2+} (10 μM) upon addition of EDTA (10 μM)

9. Fig. 8 DFT-optimized structures of (a) **PHP** and (b) **PHP**+ Cu^{2+} complex using the B3LYP/LanL2DZ method (blue atom, N; pink atom, Cu).

10. Fig. 9. Energy diagram for the reaction of **PHP** with Cu^{2+}.

11. Fig. 10 Cell viability values (%) estimated by an MTT assay versus incubation concentrations of **PHP**. RAW264.7 cells were cultured in the presence of **PHP** (0–50 μM) at 37 ^0C for 24 h.

12. Fig. 11. Fluorescence images of macrophage (RAW 264.7) cells treated with **PHP** and Cu^{2+}. (Left) Bright field image; (Middle) fluorescence image; and (Right) merged image. (Ex 346 nm, Em.380-390 nm)
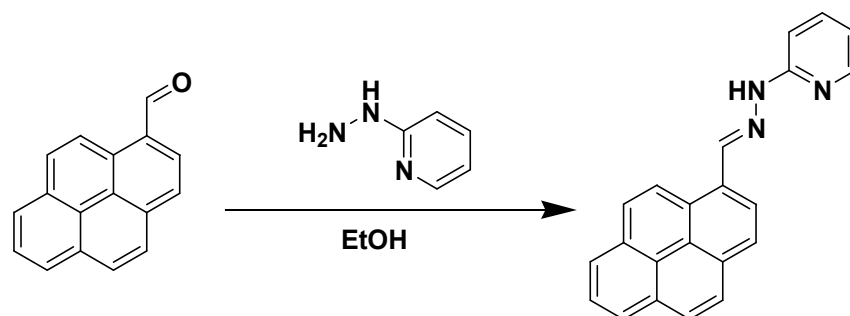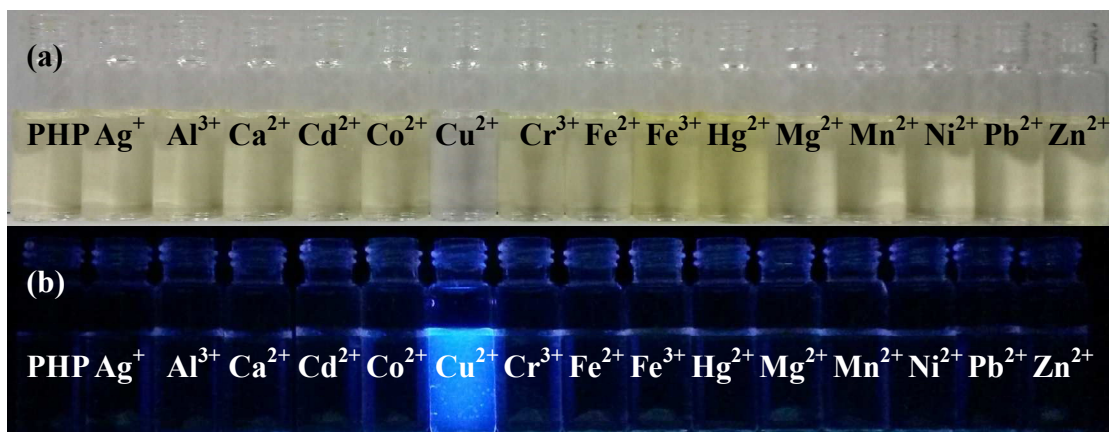
Scheme 1. Synthesis of **PHP**

Fig. 1. (a) Color and (b) fluorescence changes of **PHP** (100 µM) after addition of various metal ions (100 µM) in CH_3CN/H_2O (v/v = 4:6, 10 mM PBS, pH 7.4) solution.
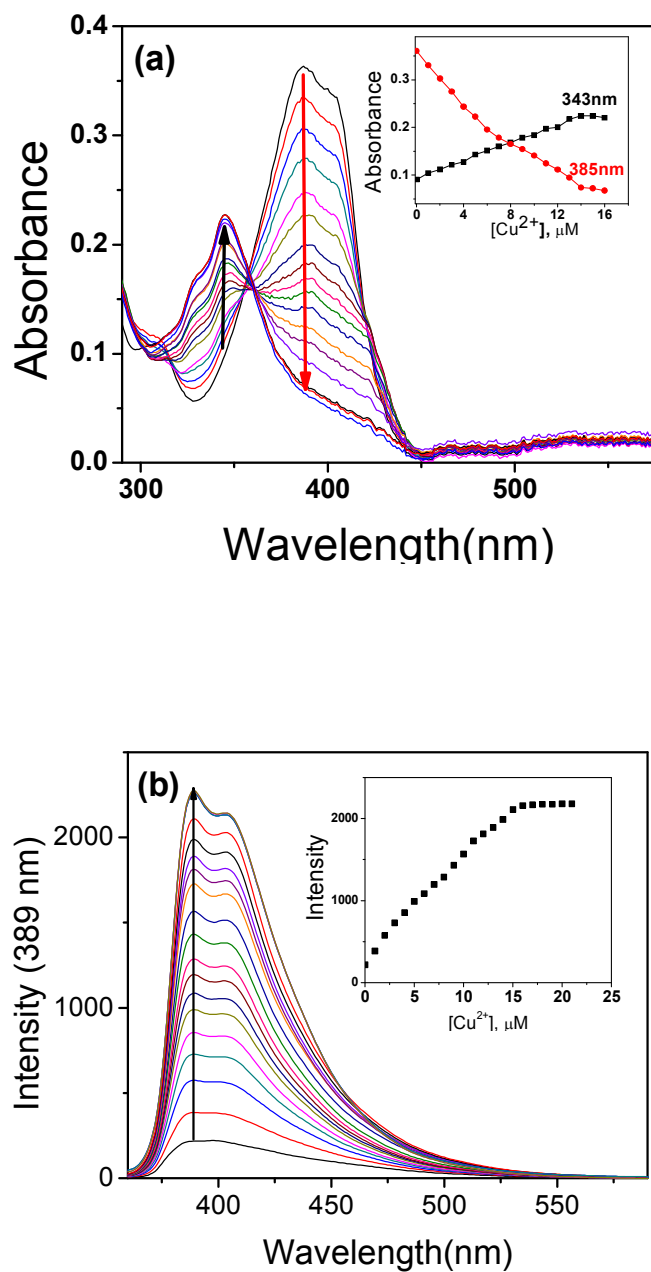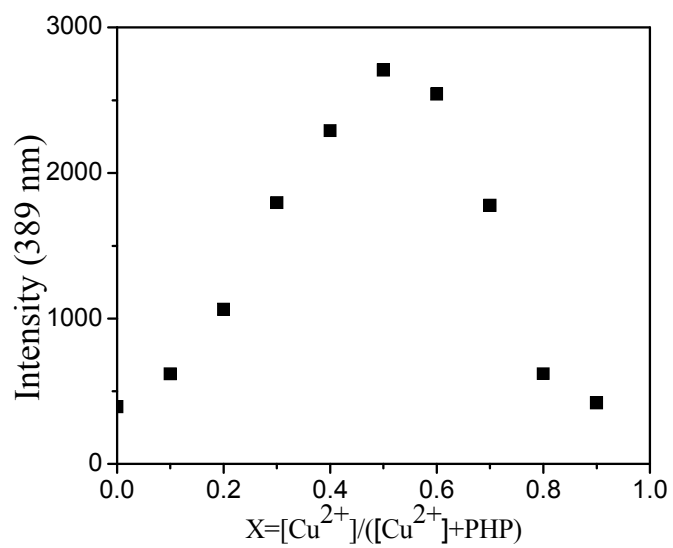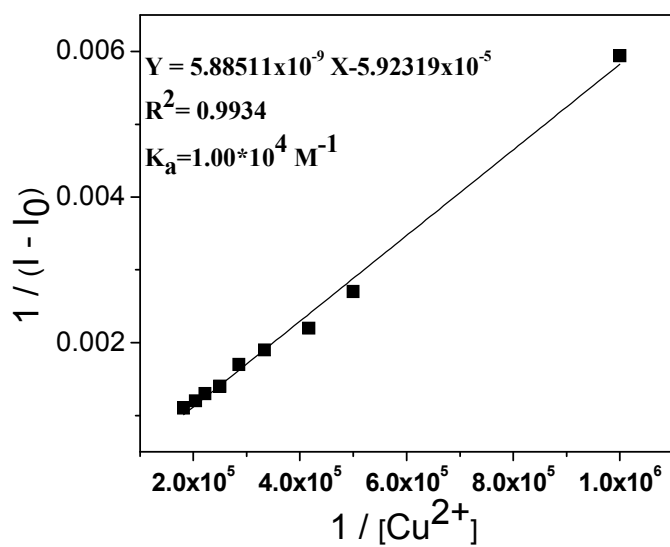
Fig. 2. (a) Absorption change and (b) fluorescence response of **PHP** (10 μM) to various equivalents of Cu^{2+} in CH_3CN/H_2O (v/v = 4:6, 10 mM PBS, pH 7.4) solution.

Fig. 3. Job plot of the Cu^{2+}-**PHP** complexes in CH_3CN/H_2O (v/v = 4:6, 10 mM PBS, pH 7.4) solution. The total concentration of **PHP** and Cu^{2+} was 50 μM. The excitation wavelength was 346 nm.

Fig. 4 Binding constant for titration of Cu^{2+} (0.1 to 1.0 eq) against ratio of fluorescence response for **PHP** (10 μM) in CH_3CN/H_2O (v/v = 4:6, 10 mM PBS, pH 7.4) solution. The excitation wavelength was 346 nm.
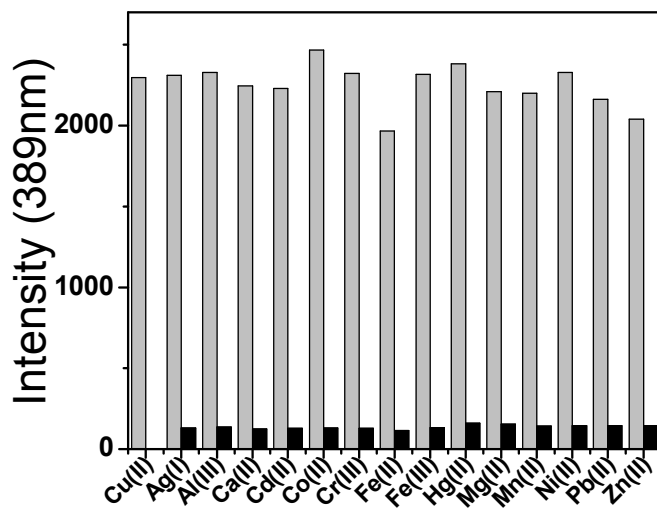
Fig. 5. Fluorescence response of **PHP** (10 µM) to Cu^{2+} (20 µM) or 100 µM of other metal ions (the black bar portion) and to the mixture of other metal ions (40 µM) with Cu^{2+} (20 µM) (the gray bar portion) in CH_3CN/H_2O (v/v = 4:6, 10 mM PBS, pH 7.4) solution.
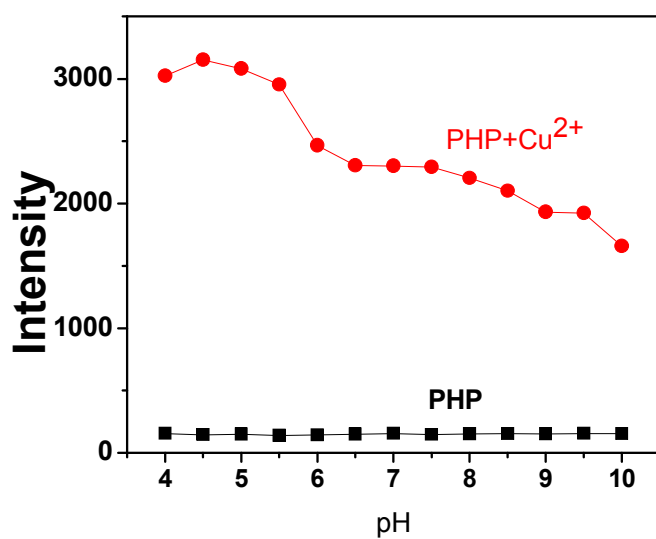
Fig. 6. Fluorescence response (389 nm) of free **PHP (**10 μM) and after addition of Cu^{2+} (10 μM) in CH_3CN/H_2O (v/v = 4:6, 10 mM PBS) solutions as a function of various pH values. The excitation wavelength was 346 nm.
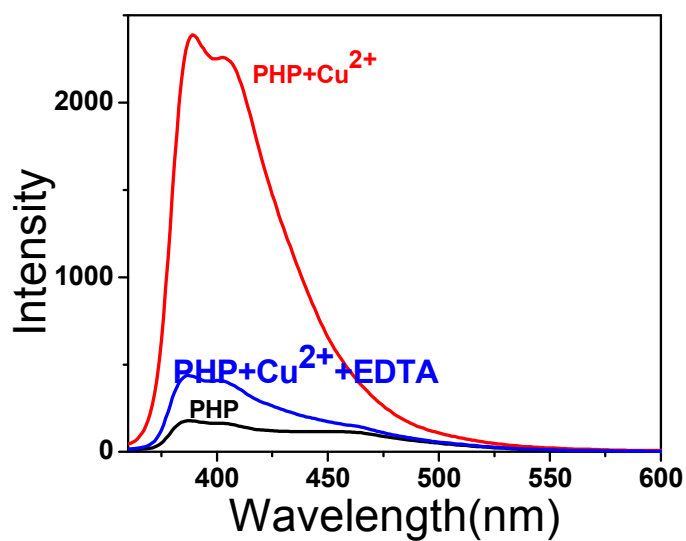
Fig. 7. Reversible binding of Cu^{2+} with **PHP**. Fluorescence spectra of (a) **PHP**, (b) **PHP** in the presence of Cu^{2+} (10 μM), and (c) probe in the presence of Cu^{2+} (10 μM) upon addition of EDTA (10 μM)

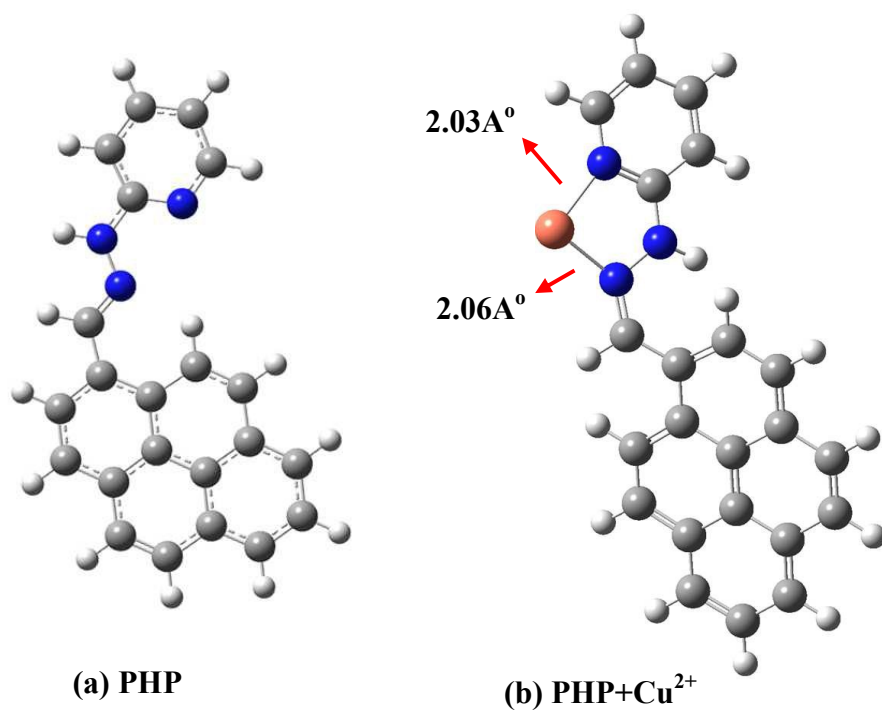**(a) PHP**   **(b) PHP+Cu^{2+}**

Fig. 8 DFT-optimized structures of (a) **PHP** and (b) **PHP**+ Cu^{2+} complex using the B3LYP/LanL2DZ method (blue atom, N; pink atom, Cu).
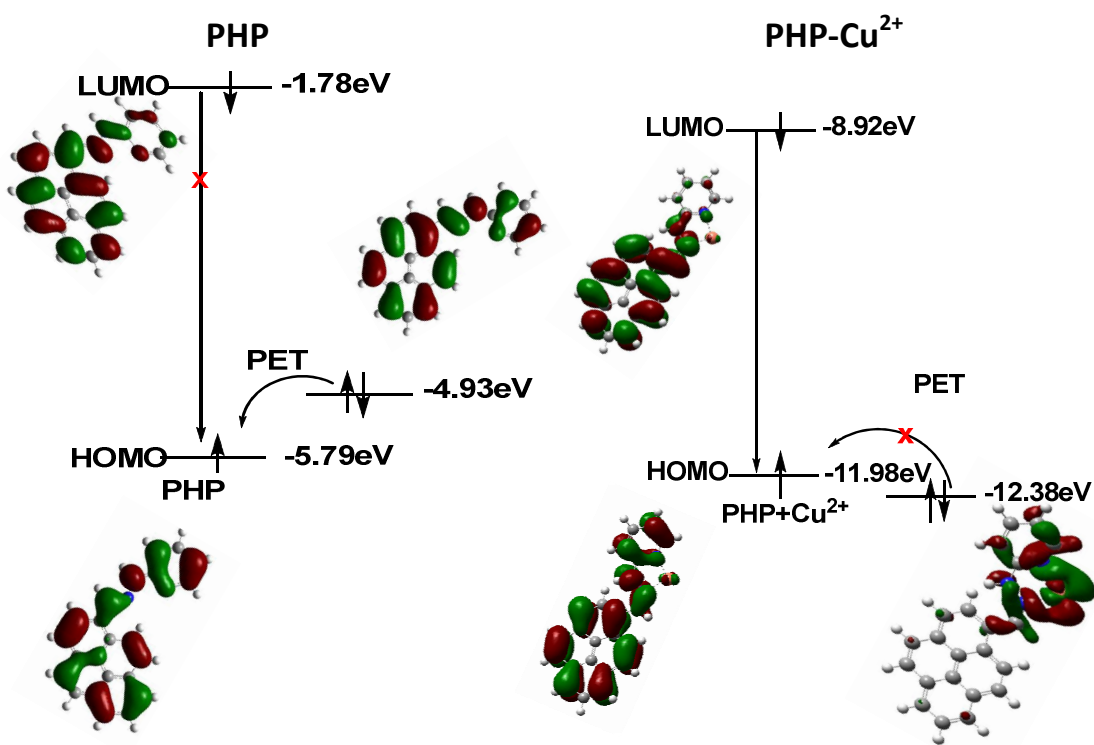
Fig. 9. Energy diagram for the reaction of **PHP** with Cu^{2+}.
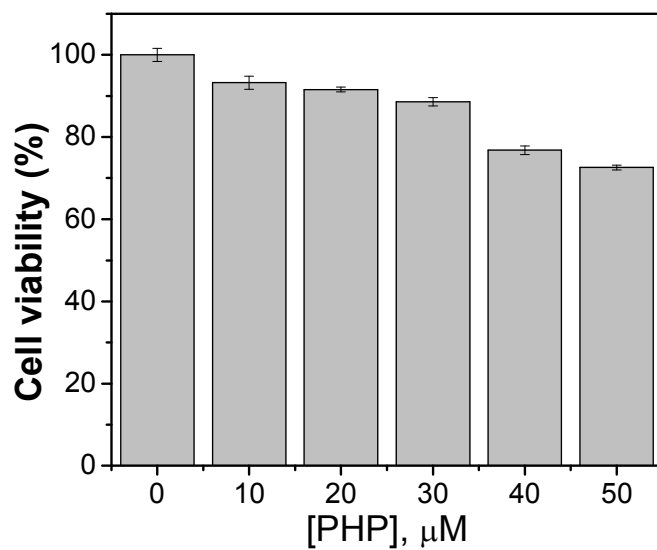
Fig. 10 Cell viability values (%) estimated by an MTT assay versus incubation concentrations of **PHP**. RAW264.7 cells were cultured in the presence of **PHP** (0–50 µM) at 37 ^{0}C for 24 h.

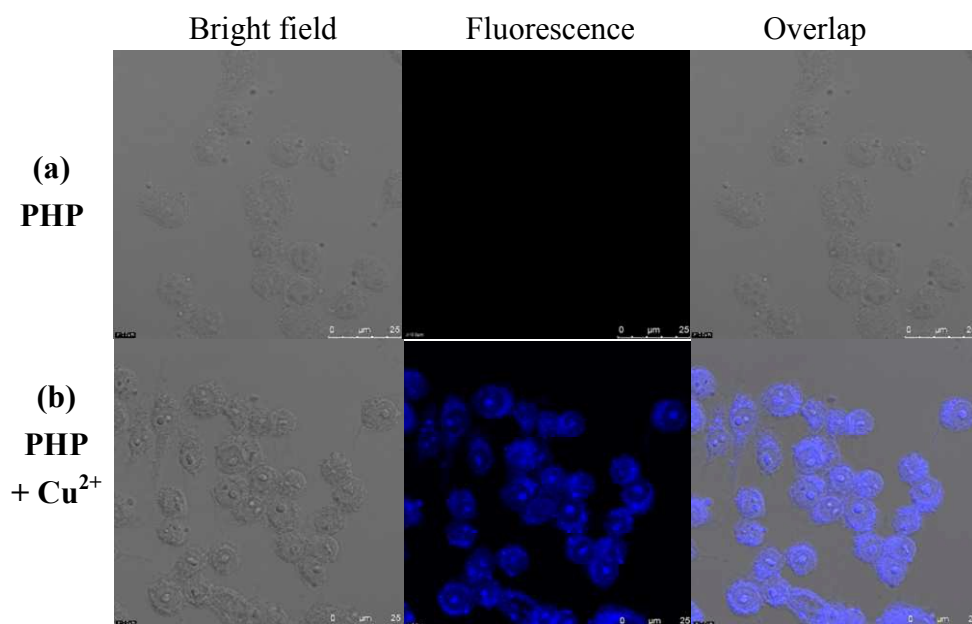| | Bright field | Fluorescence | Overlap |

**(a)
PHP**

**(b)
PHP
+ Cu^{2+}**

Fig. 11. Fluorescence images of macrophage (RAW 264.7) cells treated with **PHP** and Cu^{2+}. (Left) Bright field image; (Middle) fluorescence image; and (Right) merged image. (Ex 346 nm, Em.380-390 nm)